

TIMEREWARDER: LEARNING DENSE REWARD FROM PASSIVE VIDEOS VIA FRAME-WISE TEMPORAL DISTANCE

Anonymous authors

Paper under double-blind review

ABSTRACT

Designing dense rewards is crucial for reinforcement learning (RL), yet in robotics it often demands extensive manual effort and lacks scalability. One promising solution is to view *task progress* as a dense reward signal, as it quantifies the degree to which actions advance the system toward task completion over time. We present *TimeRewarder*, a simple yet effective reward learning method that derives progress estimation signals from passive videos, including robot demonstrations and human videos, by modeling temporal distances between frame pairs. We then demonstrate how *TimeRewarder* can supply step-wise proxy rewards to guide reinforcement learning. In our comprehensive experiments on ten challenging Meta-World tasks, we show that *TimeRewarder* dramatically improves RL for sparse-reward tasks, achieving nearly perfect success in 9/10 tasks with only 200,000 interactions per task with the environment. This approach outperformed previous methods and even the manually designed environment dense reward on both the final success rate and sample efficiency. Moreover, we show that *TimeRewarder* can exploit real-world human videos, highlighting its potential as a scalable approach path to rich reward signals from diverse video sources.

1 INTRODUCTION

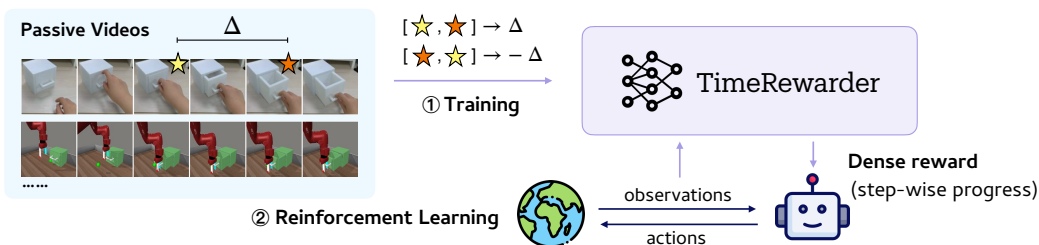


Figure 1: Overview of *TimeRewarder*. Mirroring how humans infer task progression by observing others, *TimeRewarder* distills frame-wise temporal distances from expert videos and converts them into dense reward signals, thereby enabling reinforcement learning free of manually engineered rewards or action annotations.

Reinforcement learning (RL) has long served as a principal paradigm for robotic skill acquisition (Ibarz et al., 2021; Tang et al., 2025). Yet, many of its most notable successes so far rely highly on carefully designed reward functions that are dense and task-instructive (Cheng et al., 2024; Nai et al., 2025). Designing such high-quality rewards remains labor-intensive, as they often require significant domain expertise, extensive hyperparameter tuning, or privileged access to ground-truth environments, especially for robotic manipulations (Ng et al., 1999a; Levine et al., 2016; Rajeswaran et al., 2017; Roy et al., 2021). These challenges incurred during manual reward design severely constrain the scalability of RL approaches, motivating the development of automated reward learning mechanisms that can alleviate human effort.

Dense reward function design for robotics often exploits explicit prior knowledge of the task’s typical progression, which estimates the distance between the current state and task completion, as

well as assesses whether the current action contributes to efficient task accomplishment (Todorov, 2004; Levine et al., 2016; Silver et al., 2021). Expert demonstrations provide a natural source of this progression knowledge: the temporal ordering of video frames directly reflects task advancement. Importantly, such signals can be derived even from passive videos, which are easy to obtain and require neither action annotations nor privileged supervision. As a result, automatic reward learning from passive videos can significantly expand the scalability of RL.

Building on this idea, we introduce *TimeRewarder* (Figure 1), which comprehends how the task proceeds by learning to predict *temporal distances* between arbitrary frames from action-free expert demonstrations. The temporal distance reflects the *task progress* between two frames: which frame is closer to task completion and by how much. When turning to the RL exploration phase, the predicted progress distances between adjacent frames can naturally serve as dense reward signals. The step-wise reward quantifies exactly how much the agent is advancing or regressing at each moment, guiding the agent toward accomplishing the task by implicitly imitating the expert demonstrations.

We evaluate *TimeRewarder* in the imitation-from-observation setting, where only expert videos are available and no expert action labels or dense environment rewards are provided. On 10 Meta-World (Yu et al., 2020) manipulation tasks with 100 demonstrations per task, *TimeRewarder* surpasses all baselines on 9 tasks in both success rate and sample efficiency. This performance gain highlights the high quality of the reward produced by *TimeRewarder*: it effectively assigns credits to partial progress and penalizes unproductive behaviors even on out-of-distribution transitions along the agent trajectories, thus providing strong instructive guidance to the RL process.

2 RELATED WORKS

Previous work has explored methods of learning from observation-only demonstrations, providing agents with task-relevant supervision when environmental rewards are sparse or inaccessible.

Action recovery. Model-based approaches (Nair et al., 2017; Torabi et al., 2018a; Pathak et al., 2018; Edwards et al., 2019; Radosavovic et al., 2021; Fan et al., 2022; Baker et al., 2022; Liu et al., 2022; Ramos et al., 2023) attempt to recover missing actions in expert demonstrations by training inverse dynamics models from online exploration data, and apply behavioral cloning on annotated videos. However, these methods necessitate the collection of vast amounts of transition data to train reliable action-recovery models, and this training must be performed iteratively online to ensure the state distribution of the expert demonstrations is adequately covered. Such a delicate and unstable process limits their practical deployment in potential real-world robotic scenarios.

Inverse RL. Instead of explicitly recovering actions for behavior cloning, Inverse RL aims to build reward functions from expert demonstrations (and online interactions if needed) to guide policy updates within a standard RL paradigm. Trajectory-matching methods (Dadashi et al., 2020; Yang et al., 2019; Jaegle et al., 2021; Chen et al., 2021; Haldar et al., 2023; Liu et al., 2024) measure rollout-expert similarity as a reward signal, while adversarial imitation learning (Ho & Ermon, 2016; Torabi et al., 2018b; Cai et al., 2019) trains a discriminator to distinguish agent from expert transitions. With the advance of generative models, some recent works (Escontrela et al., 2023; Huang et al., 2024) train video generation models and take the likelihood of rollout frames produced by this model as the reward. Despite the progress of these methods, they face challenges such as high online computational cost (Haldar et al., 2023; Escontrela et al., 2023), training instability (Ho & Ermon, 2016), or reward hacking (Escontrela et al., 2023).

Progress-based reward learning. Within inverse RL, some methods define proxy rewards by exploiting the temporal structure of demonstrations, where the ordering of frames along a trajectory provides an implicit measure of *task progress*. TCC (Dwibedi et al., 2019) enforces cycle-consistency in time for correspondence, while Arrow of Time (Wei et al., 2018) exploits temporal irreversibility for representation learning. TCN (Sermanet et al., 2018) pulls temporally adjacent frames together in the latent visual representation space while pushing distant ones apart. However, as pointed out by Ma et al. (2022), standard TCN enforces only coarse temporal consistency and produces non-locally smooth representations. Building on this, VIP (Ma et al., 2022) estimates frame-goal distances using implicit time-contrastive learning. However, we found this objective difficult to optimize reliably. GVL (Ma et al., 2024) uses vision-language models to infer temporal orders from shuffled frames, yet we observed that the outputs of these large models can be

inconsistent, limiting their effectiveness in building reward functions. Rank2Reward (Yang et al., 2024) learns to predict the temporal order of adjacent frame pairs, providing lightweight local rewards; PROGRESSOR (Ayalew et al., 2024) considers triples of frames to estimate the relative position of an intermediate frame between start and goal states. However, both Rank2Reward and PROGRESSOR report that rewards trained solely on expert data tend to overestimate progress for out-of-distribution states, necessitating online refinement for stable policy learning.

In contrast, our method directly estimates *frame-wise temporal distances*, producing more accurate and stable proxy rewards. Once trained on expert videos, the reward model can be frozen during RL, eliminating the need for online updates. These properties enable its potential scaling to large and diverse demonstration datasets, making it better suited for practical policy learning.

3 PRELIMINARIES

3.1 LEARNING FROM ACTION-FREE DEMONSTRATIONS

We study the problem of learning policies from action-free expert demonstrations. Specifically, the agent has access to a dataset of expert RGB videos besides an environment to interact with. We resolve the problem from the RL perspective, by deriving a proxy reward from the action-free demonstrations, which is used to guide downstream policy optimization.

Formally, we consider an agent interacting with a finite-horizon Markov Decision Process $(\mathcal{S}, \mathcal{A}, \mathcal{P}, \mathcal{R}, \gamma, T)$, where \mathcal{S} is the state space, \mathcal{A} the action space, \mathcal{P} the transition dynamics, \mathcal{R} the reward function, γ the discount factor, and T the horizon. We assume the agent can not access states $s_t \in \mathcal{S}$ directly, but only high-dimensional visual observations $o_t \in \mathcal{O}$ in the form of RGB images. Moreover, the environmental reward function \mathcal{R} provides only sparse binary success signals indicating whether the task is completed or not, which is easily obtainable via human annotation or vision-language model API.

Such sparse signals are far from enough for guiding efficient policy optimization. To overcome this, we derive a proxy reward from the expert data, hoping that the agent can receive instructive learning signals even when the environmental reward remains zero during exploration. We denote the expert dataset as $D^e = \{\tau_i^e\}$, where $\tau^e = (o_1^e, o_2^e, \dots, o_T^e)$ represents observation trajectories. The goal is to recover a proxy reward function $\hat{\mathcal{R}}$ from D^e , such that a policy $\pi^{\hat{\mathcal{R}}}$ trained on this reward:

$$\pi^{\hat{\mathcal{R}}} = \arg \max_{\pi} \mathbb{E} \left[\sum_{t=1}^T \gamma^{t-1} \hat{\mathcal{R}}(o_t, o_{t+1}) \right] \quad (1)$$

can successfully accomplish the task.

3.2 PROGRESS-BASED REWARD DESIGN

Since the agent’s ultimate objective is to reach a goal state, the distance to task completion can be interpreted as a measure of task progress, which can inform reward design. This idea is closely related to potential-based reward shaping (Ng et al., 1999b), where the reward at each transition is defined as the change in a potential function $V(o)$ that measures progress from o toward the goal:

$$r_t = \hat{\mathcal{R}}(o_t, o_{t+1}) = V(o_t) - \gamma V(o_{t+1}). \quad (2)$$

Such progress-based proxy rewards offer two primary benefits: (1) *Generality*: Task progress is a high-level signal that is implicitly encoded in expert demonstrations, avoiding the need for hand-crafted reward design. (2) *Action-free learning*: Progress can be inferred directly from passive video data, without requiring access to action labels. These properties yield dense and temporally consistent feedback, enabling policy learning from action-free video demonstrations.

4 METHOD

We introduce *TimeRewarder*, a framework that derives dense proxy rewards for downstream RL by estimating task progress from action-free expert videos. The central idea is to model progress as

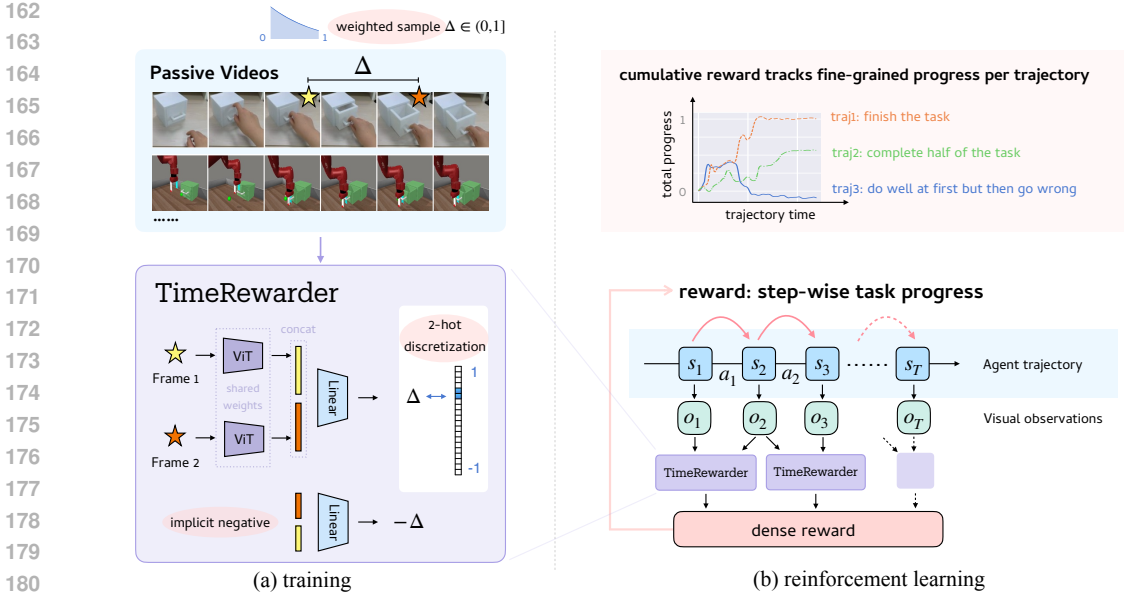


Figure 2: *TimeRewarder* framework. *TimeRewarder* learns step-wise dense rewards from passive videos by modeling intrinsic temporal distances, enabling robust progress scoring that assigns high values to states reflecting task advancement, while penalizing suboptimal actions lacking meaningful contribution to task progression, thereby facilitating effective policy learning.

a *temporal distance prediction problem*: learning to estimate the temporal distance between two observations in a trajectory. In this section, we (1) formalize the construction and training of *TimeRewarder*, (2) present its application in deriving reward functions for RL, and (3) provide a theoretical justification demonstrating that temporal distance aligns naturally with task progress.

4.1 TRAINING WITH FRAME-WISE TEMPORAL DISTANCE

We train *TimeRewarder*, a progress model $F_\theta : \mathcal{O} \times \mathcal{O} \rightarrow \mathbb{R}$, on expert demonstrations D^e . The model learns to predict the normalized temporal distance between two ordered frames (o_u^e, o_v^e) , providing a dense signal of task progress. As shown in Figure 2 (a), given two frames (o_u^e, o_v^e) from an expert trajectory, their normalized temporal distance is computed as:

$$d_{uv} = \frac{v - u}{T - 1} \in [-1, 1], 1 \leq u, v \leq T, \tag{3}$$

so that F_θ is trained in a self-supervised manner, taking two ordered frames and predicting the relative temporal distance between them.

To be effective as a reward signal, F_θ must satisfy two key principles: (1) **Suboptimality Awareness** — generalize beyond expert data and assign lower scores to suboptimal behaviors which are unseen in D^e ; (2) **Fine-grained Temporal Resolution** — capture fine-grained progress, particularly between adjacent steps.

For *suboptimal awareness*, *TimeRewarder* naturally realize **Implicit Negative Sampling**: the frame indices u and v in equation 3 can appear in either forward or backward order, so the normalized temporal distance d_{uv} ranges from -1 to 1 . A positive value indicates forward progression toward the goal, while a negative value indicates backward progression, naturally corresponding to movement away from task completion, simulating suboptimal or incorrect behaviors. This formulation imposes an antisymmetric structure on the learning objective, thereby discouraging trivial memorization shortcuts (Ma et al., 2024).

As for *fine-grained temporal resolution*, we aim to enhance the model’s ability to recognize progress at the step level, i.e., between adjacent frames, so that the learned metric can provide reliable step-wise rewards. To this end, we introduce **Exponentially Weighted Pair Sampling**: the temporal

interval $\Delta = |v - u|$ in a frame pair (o_u^e, o_v^e) is sampled according to

$$P(\Delta) \propto \exp(-\lambda\Delta), \quad \Delta \in \{1, \dots, T - 1\}, \quad (4)$$

where $\lambda > 0$ controls the bias toward shorter intervals while still ensuring coverage of longer horizons. This sampling scheme emphasizes fine-grained local differences while retaining the ability to capture broader temporal dependencies.

Besides, to ensure numerical stability and maintain accuracy during the optimization process, we employ **Two-hot Discretization** (Wang et al., 2024) to discretize the scalar temporal distance $d_{uv} \in [-1, 1]$. Specifically, the target range $[-1, 1]$ is uniformly partitioned into K bins (we set $K = 20$ by default). For a given d_{uv} , we compute a soft two-hot distribution $\mathbf{y}_{uv} = \Phi(d_{uv}) \in \mathbb{R}^K$ that assigns non-zero mass only to the two nearest bins. The progress model F_θ outputs a logit vector $\hat{\mathbf{y}}_{uv} = F_\theta(o_u^e, o_v^e) \in \mathbb{R}^K$, and the training objective is the cross-entropy loss:

$$\min_{\theta} \mathbb{E}[-\mathbf{y}_{uv}^\top \log \text{softmax}(\hat{\mathbf{y}}_{uv})]. \quad (5)$$

Through this training, F_θ learns a robust notion of temporal progress inside any ordered frame pairs from purely observational passive video data.

4.2 POLICY LEARNING WITH TEMPORAL DISTANCE REWARD

Then, we utilize F_θ to provide dense proxy rewards for RL. As illustrated in Fig. 2 (b), for each policy rollout, *TimeRewarder* computes adjacent frame distances as step-wise rewards:

$$r_{\text{TR}}(o_t, o_{t+1}) = \hat{d}_{t,t+1} = \Phi^{-1}[F_\theta(o_t, o_{t+1})] \in [-1, 1], \quad (6)$$

where the output logits of F_θ have been converted back to a scalar value.

During policy optimization, we combine this progress-based dense reward with a sparse success signal:

$$r_t = r_{\text{TR}}(o_t, o_{t+1}) + \alpha \cdot r_{\text{success}}(o_t), \quad (7)$$

where $r_{\text{success}} : \mathcal{O} \rightarrow \{0, 1\}$ is a binary success indicator (1 if successful, 0 otherwise), and $\alpha \geq 0$ is a weight constant.

Although F_θ is trained solely on expert trajectories, its design ensures natural generalization to diverse behaviors. Suboptimal behaviors—such as stalls, loops, or regressions—receive lower or even negative rewards, while meaningful partial progress is still recognized and positively rewarded. This graded, step-wise feedback provides informative signals for exploration, guiding the agent to recover from failures and make constructive progress toward task completion. Together with the sparse success signal, this mechanism allows *TimeRewarder* to produce dense and informative rewards throughout training, which underlies its empirical effectiveness demonstrated in Section 5.

4.3 THEORETICAL JUSTIFICATION

We provide a theoretical justification for our motivation that the task progress in expert videos can be formalized in terms of temporal distance. For each expert trajectory $\tau^e = (o_1^e, \dots, o_T^e)$, we treat the final frame as the goal observation o_g^e . If the true reward is absent, the normalized step cost can be approximated as $\frac{1}{T-1}$, where T is the trajectory length. The progress (potential) of each observation o_t^e can thus be expressed as:

$$V(o_t^e) = \mathbb{E} \left[\sum_{k=t}^{T-1} \frac{1}{T-1} \gamma^{k-t} \mathbf{1}\{o_k^e \neq o_g^e\} \right], \quad V(o_g^e) = 0, \quad (8)$$

where $\mathbf{1}\{\cdot\}$ denotes the indicator function.

Under the assumption of expert optimality, this potential satisfies the Bellman equation.

$$V(o_t^e) = \mathbb{E} \left[\frac{1}{T-1} + \gamma V(o_{t+1}^e) \right]. \quad (9)$$

Generally, γ is set to a large value close to 1, so along the expert trajectory, the progress reward in equation 2 approximates the per-step temporal distance $\frac{1}{T-1}$. This highlights that frame-wise temporal distance provides a natural and theoretically motivated measure of progress.

270 5 EXPERIMENTS

271
272 In this section, we assess the performance of *TimeRewarder*. We present the experiment setup,
273 evaluate *TimeRewarder* against baselines, and do ablation studies of its key components.

274 5.1 EXPERIMENT SETUP

275
276
277 **Evaluation Benchmark.** We evaluate *TimeRewarder* and other methods on ten challenging Meta-
278 World (Yu et al., 2020) manipulation tasks (see Appendix A.1 for details). For each task, we provide
279 100 action-free expert videos generated by Meta-World’s scripted policies. For three tasks among
280 them, we further consider a cross-domain setting where only one in-domain expert video is provided
281 per task, supplemented with 20 real-world human demonstration videos.

282 **Implementation Details.** We use a CLIP-pretrained ViT-B (Radford et al., 2021; Dosovitskiy et al.,
283 2021) as the visual backbone of *TimeRewarder*. During training, frame pairs are independently
284 encoded, concatenated, and passed through a linear layer to predict discretized temporal distances.
285 Both the ViT-B encoder and linear layer are trainable. For RL, *TimeRewarder* is integrated with
286 DrQ-v2 (Yarats et al., 2021), and the whole network is frozen, providing dense step-wise rewards
287 from adjacent observation frames. See Appendix A.4.3 for hyperparameters.

288 **Baselines.** We compare *TimeRewarder* against eight baselines, grouped into three categories:

- 289 1. *Progress-Based Reward Learning:* **PROGRESSOR** (Ayalew et al., 2024) fits a Gaus-
290 sian model to estimate relative frame positions between initial and goal as rewards;
291 **Rank2Reward** (Yang et al., 2024) estimates temporal rank between frames as rewards; and
292 **VIP** (Ma et al., 2022) trains an implicit value model to estimate task progress of each frame.
293 For fair comparison, following their settings, goal frames sampled from expert videos are pro-
294 vided to PROGRESSOR and VIP.
- 295 2. *Imitation Learning from Observations:* **GAIfO** (Torabi et al., 2018b), **OT** (Papagiannis &
296 Li, 2022), and **ADS** (Liu et al., 2024) compute rewards online by comparing rollouts to ex-
297 pert videos. GAIfO uses a discriminator, OT applies Wasserstein distance via Optimal Trans-
298 port (Villani et al., 2009), and ADS extends OT with curriculum scheduling on the discount
299 factor to better handle progress-dependent tasks.
- 300 3. *Privileged Methods:* For reference, we also report results of policies with access to privileged
301 information: **BC** (Bain & Sammut, 1995) trains a behavior cloning policy with expert actions,
302 and **Environment reward** uses Meta-World’s ground-truth dense reward.

303
304 For the seven baselines involving reinforcement learning (except **BC**), we uniformly adopt DrQ-
305 v2 (Yarats et al., 2021) as the underlying RL algorithm for fair comparison.

306 5.2 PERFORMANCE OF TIMEWARDER

307
308 We address the following four questions to structure our experimental results and analysis, to demon-
309 strate the superior performance achieved by *TimeRewarder* against the baselines.

310 **Question 1.** *Does TimeRewarder provide correct task progress for unseen success trajectories*
311 *rather than relying on memorization?*

312
313 A well-shaped reward should encourage successful rollouts with monotonic progress, even when
314 trajectories differ from training demonstrations in object positions or motion paths. We test
315 *TimeRewarder* and progress-based reward baselines under the Value-Order Correlation (VOC) met-
316 ric (Ma et al., 2024), which evaluates the alignment between predicted values and temporal order
317 (+1 for perfect monotonicity increasing, 0 for no correlation, -1 for inverse). Specifically, we
318 train *TimeRewarder* and VIP on 100 expert demonstrations and test them on 100 held-out expert
319 videos. To further strengthen the empirical comparison, we introduce GVL (Ma et al., 2024) im-
320 plemented with Gemini-1.5-Pro (Team et al., 2024) as an additional baseline, where we follow
321 its few-shot setting by giving 5 expert videos as context and another 5 for testing, where 32 frames
322 are uniformly sampled from each video. Rank2Reward and PROGRESSOR are excluded due to
323 a lack of value functions indicating progress. As shown in Figure 3, *TimeRewarder* consistently
achieves the highest VOC scores, confirming its strong temporal coherence and generalization to
unseen trajectories.

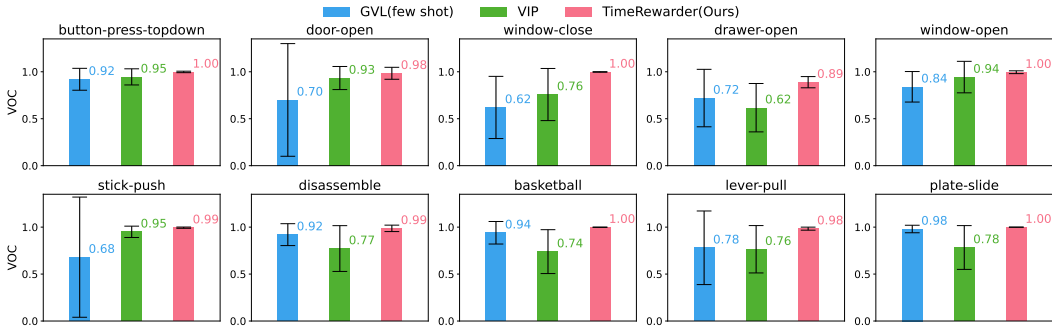


Figure 3: Value-Order Correlation (VOC) on held-out expert videos. Higher is better.

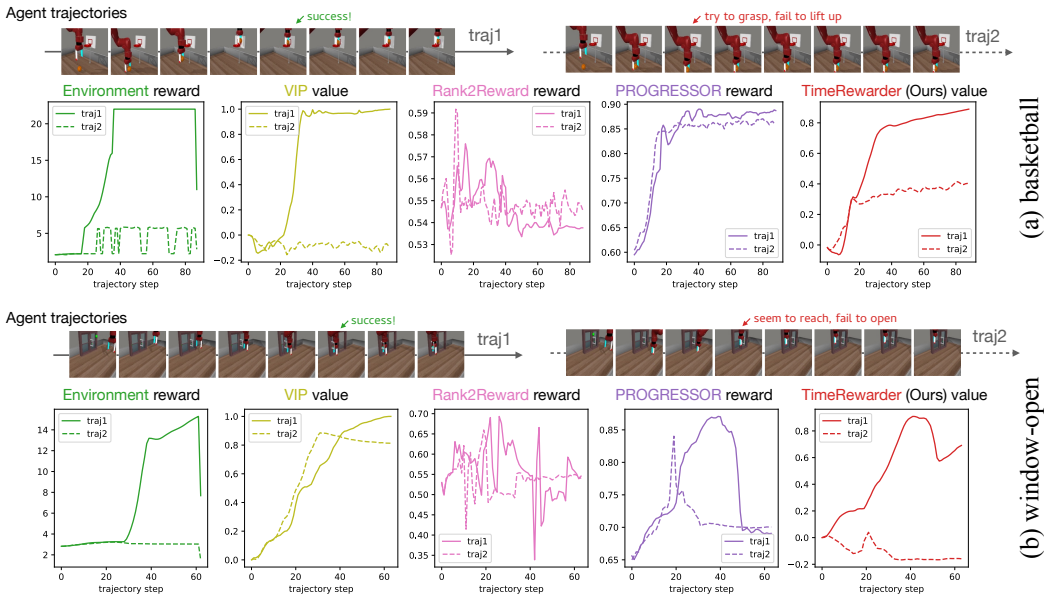


Figure 4: Reward/value curves on successful ($traj_1$) vs. failed ($traj_2$) rollouts for two tasks. *TimeRewarder* and VIP output values (cumulative progress), PROGRESSOR outputs step-wise rewards, while Rank2Reward is visualized through its pairwise ordering reward signals. *TimeRewarder* provides the most informative and temporally coherent feedback.

Question 2. Can *TimeRewarder* identify suboptimal behavior in rollout trajectories?

Reward models trained on demonstrations of only successful behaviors inevitably face out-of-distribution transitions during RL exploration, where they may misinterpret them by either overestimating failures or undervaluing successes. We select one representative successful ($traj_1$) and one failed ($traj_2$) trajectory from two tasks, and visualize the progress estimates of *TimeRewarder* against three baselines in Figure 4.

In the *basketball* task, where $traj_2$ grasps but never lifts the ball, VIP ignores partial progress and PROGRESSOR saturates after grasping, while *TimeRewarder* cleanly captures half-success and then separates completion from failure. In the *window-open* task, where $traj_2$ mimicks opening motions midair without contacting the handle, VIP is misled by visual similarity and PROGRESSOR gives spurious early spikes which can mislead exploration, whereas *TimeRewarder* increases values only upon meaningful interaction. Rank2Reward, limited to pairwise orderings, fails to produce consistent distinctions. These comparative results demonstrate *TimeRewarder*'s unique capacity for temporally coherent and causally grounded feedback under distribution shift—significantly outperforming previous methods in distinguishing productive from unproductive behaviors.

Question 3. Can *TimeRewarder* improve reinforcement learning performance?

We present the downstream RL performance of *TimeRewarder* against baselines in Figure 5. Specifically, we implement DrQ-v2 with rewards summed up from the proxy rewards produced by

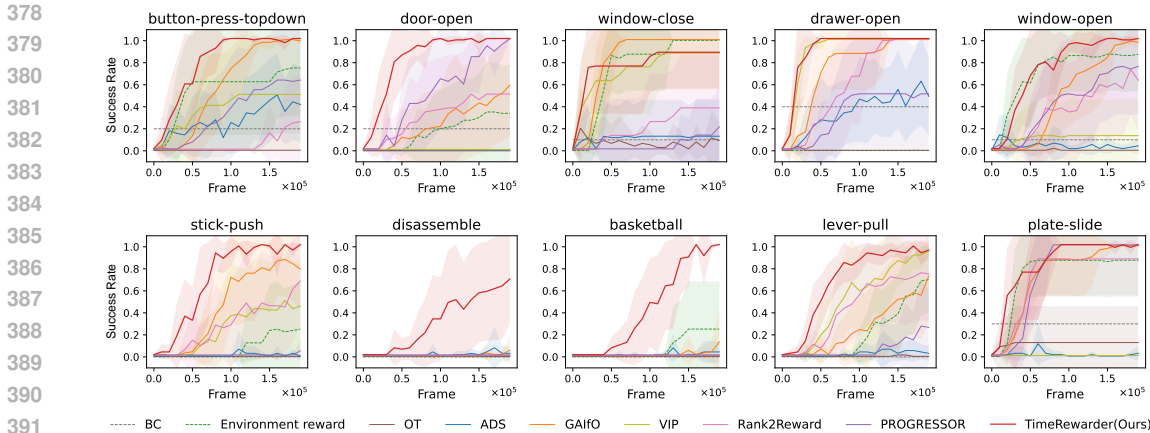


Figure 5: Performance of reinforcement learning with sparse environment success signals and dense proxy rewards from each method. Curves show mean \pm s.d. over eight seeds. Dashed lines indicate reference settings of behavior cloning (BC) and environment dense reward supervision.

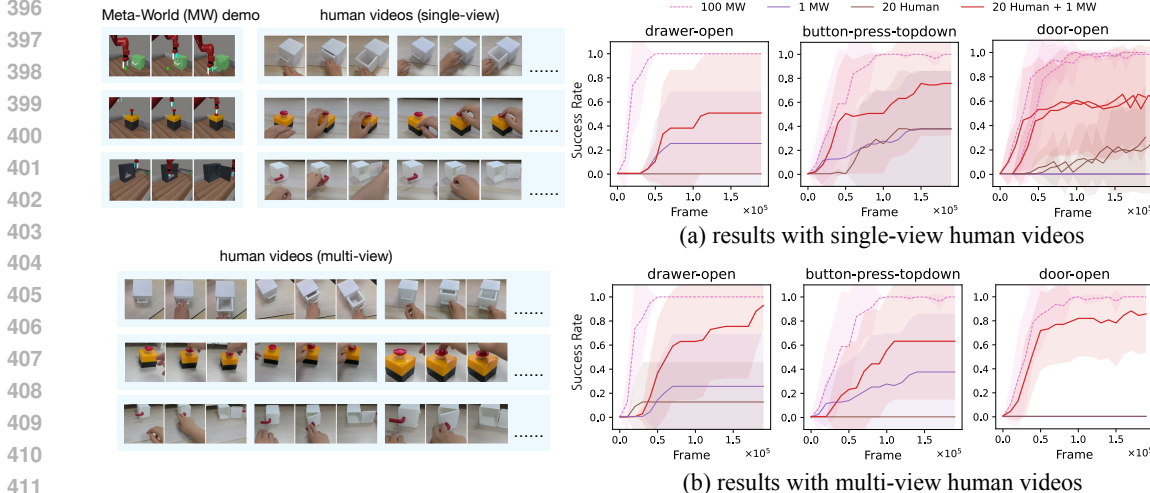


Figure 6: Cross-domain reward learning. *TimeRewarder* improves performance by leveraging 20 unlabeled human videos alongside only 1 in-domain Meta-World demonstration per task, demonstrating its ability to utilize cross-domain visual data. Curves show mean \pm s.d. over eight seeds.

these methods and the environmental binary success signals, similar to equation 7. We see that *TimeRewarder* attains the highest final success rate and the greatest sample efficiency on 9 of 10 tasks. Remarkably, *TimeRewarder* also outperforms policies trained with dense **Environment reward** on 9 tasks, which is commonly treated as an upper bound. These results demonstrate that *TimeRewarder*, a progress-based reward learning method, not only eliminates the need for manual reward design but can even surpass it in effectiveness. Additional experiments without environment success signals are provided in Appendix A.3.2.

Question 4. *Can TimeRewarder generalize across different domains and even embodiments?*

To test cross-domain generalization, we choose 3 tasks and build their corresponding copies in real-world. For these 3 tasks we collect 20 human demonstrations individually under each of the following 2 camera settings: fixed viewpoint or varying viewpoints. Such cross-domain videos, together with a single in-domain expert video from the original Meta-World environment, are then provided to *TimeRewarder* for reward learning and downstream RL. As shown in Figure 6, training on either human-only (brown) or Meta-World-only (purple) data yields low success rates, but combining them (red) substantially improves performance. These results highlight the ability of *TimeRewarder* to leverage cross-domain, unlabeled video data for reward learning, even when in-domain supervision is scarce. The full set of human videos is shown in Appendix A.2.

5.3 ABLATION STUDIES

In Figure 7, we evaluate the contribution of each methodological component in Section 4.1 through controlled removals:

Effect of Implicit Negative Sampling: Implicit negative sampling enforces *suboptimal awareness* by treating reverse-ordered frame pairs as implicit negatives, simulating failures during training. Removing it and predicting only forward progress $\in [0, 1]$ causes sharp drops in *stick-push* and *basketball* (orange line), where failed grasps must be penalized. Without negatives, the model overestimates such failures as partial success. PROGRESSOR, which also lacks this mechanism, similarly collapses (Figure 5), highlighting its necessity.

Effect of Weighted Sampling: Weighted sampling enforces *fine-grained temporal resolution* by emphasizing short frame intervals while still covering long horizons. Replacing it with uniform sampling reduces performance in *stick-push* and *window-open* (pink line), where precise interactions are required. Without focusing on adjacent frames, the model misses subtle cues, yielding ambiguous rewards that fail to guide effective, precise action learning.

Effect of Discretization: Two-hot discretization ensures *numerical stability* and sharp progress boundaries by binning temporal distances. Replacing it with direct regression causes large drops in *basketball* and *disassemble* (purple line), where long setup phases are followed by brief decisive actions (e.g., lifting the ball or ring). Direct regression smooths over these moments, failing to distinguish success from near-success, while discretization preserves sharp transitions and provides stronger completion incentives.

We also evaluate three alternative designs (details in Appendix A.4.1): (1) **only from init** measures progress only relative to the initial frame; (2) **single frame input** predicts the progress of each single frame instead of relative progress between two frames; and (3) **order prediction** is inspired by GVL (Ma et al., 2024) and reconstructs sequences from shuffled frames. All perform worse: the former two settings lack temporal expressiveness, while the third one adds complexity without benefit, underscoring the effectiveness of *TimeRewarder*.

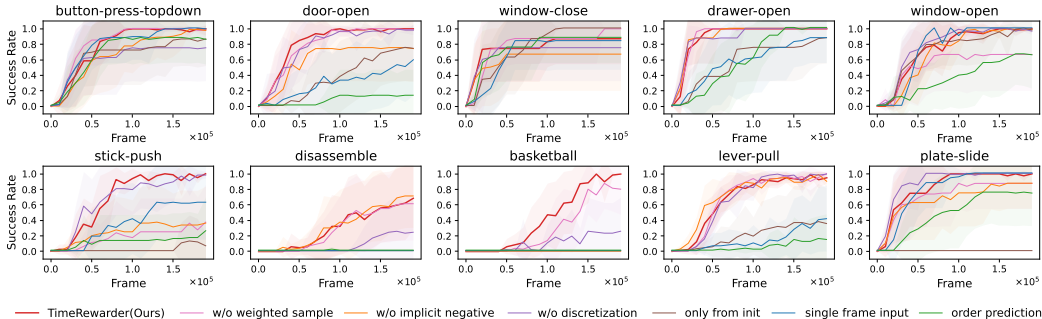


Figure 7: Ablation study results. Curves show mean \pm s.d. over eight seeds.

6 CONCLUSION

We present *TimeRewarder*, a simple yet effective method that produces dense instructive rewards by learning to predict temporal distances from action-free expert videos. This approach captures fine-grained task progress, naturally accounts for suboptimal behaviors, and provides informative step-wise feedback for RL. Experiments on diverse robotic manipulation tasks demonstrate that *TimeRewarder* not only outperforms prior reward learning methods but also surpasses environment-supplied dense rewards, in terms of both success rate and sample efficiency. Besides, *TimeRewarder* showed successful cross-domain learning ability by leveraging real-world human videos to improve policy learning, when in-domain data is limited.

In a word, *TimeRewarder* provides a promising direction for reducing reliance on manual reward engineering. Although current limitations emerge on tasks with frequent back-and-forth motions, we expect them to be addressed by future hierarchical or memory-augmented progress models, so that scalable “watch-to-act” skill acquisition from in-the-wild video becomes truly attainable.

486 REPRODUCIBLE STATEMENT
487

488 With the code attached in our supplementary materials and the hyperparameter settings in Ap-
489 pendix A.4.3, the experiment results are highly reproducible. We also utilize sufficient random
490 seeds in Section 5 to ensure reproducibility.
491

492 REFERENCES
493

494 Tewodros Ayalew, Xiao Zhang, Kevin Yuanbo Wu, Tianchong Jiang, Michael Maire, and Matthew R
495 Walter. Progressor: A perceptually guided reward estimator with self-supervised online refine-
496 ment. *arXiv preprint arXiv:2411.17764*, 2024.
497

498 Michael Bain and Claude Sammut. A framework for behavioural cloning. In *Machine Intelligence*
499 *15*, pp. 103–129, 1995.
500

501 Bowen Baker, Ilge Akkaya, Peter Zhokov, Joost Huizinga, Jie Tang, Adrien Ecoffet, Brandon
502 Houghton, Raul Sampedro, and Jeff Clune. Video pretraining (vpt): Learning to act by watching
503 unlabeled online videos. *Advances in Neural Information Processing Systems*, 35:24639–24654,
504 2022.

505 Xin-Qiang Cai, Yao-Xiang Ding, Yuan Jiang, and Zhi-Hua Zhou. Imitation learning from pixel-level
506 demonstrations by hashreward. *arXiv preprint arXiv:1909.03773*, 2019.
507

508 Annie S Chen, Suraj Nair, and Chelsea Finn. Learning generalizable robotic reward functions from”
509 in-the-wild” human videos. *arXiv preprint arXiv:2103.16817*, 2021.

510 Xuxin Cheng, Kexin Shi, Ananye Agarwal, and Deepak Pathak. Extreme parkour with legged
511 robots. In *2024 IEEE International Conference on Robotics and Automation (ICRA)*, pp. 11443–
512 11450. IEEE, 2024.
513

514 Robert Dadashi, Léonard Hussenot, Matthieu Geist, and Olivier Pietquin. Primal wasserstein imita-
515 tion learning. *arXiv preprint arXiv:2006.04678*, 2020.

516 Alexey Dosovitskiy, Lucas Beyer, Alexander Kolesnikov, Dirk Weissenborn, Xiaohua Zhai, Thomas
517 Unterthiner, Mostafa Dehghani, Matthias Minderer, Georg Heigold, Sylvain Gelly, et al. An im-
518 age is worth 16x16 words: Transformers for image recognition at scale. *International Conference*
519 *on Learning Representations (ICLR)*, 2021.
520

521 Debidatta Dwibedi, Yusuf Aytar, Jonathan Tompson, Pierre Sermanet, and Andrew Zisserman. Tem-
522 poral cycle-consistency learning. In *Proceedings of the IEEE/CVF conference on computer vision*
523 *and pattern recognition*, pp. 1801–1810, 2019.
524

525 Ashley Edwards, Himanshu Sahni, Yannick Schroecker, and Charles Isbell. Imitating latent policies
526 from observation. In *International conference on machine learning*, pp. 1755–1763. PMLR, 2019.

527 Alejandro Escontrela, Ademi Adeniji, Wilson Yan, Ajay Jain, Xue Bin Peng, Ken Goldberg, Young-
528 woon Lee, Danijar Hafner, and Pieter Abbeel. Video prediction models as rewards for reinforce-
529 ment learning. *Advances in Neural Information Processing Systems*, 36:68760–68783, 2023.
530

531 Linxi Fan, Guanzhi Wang, Yunfan Jiang, Ajay Mandlkar, Yuncong Yang, Haoyi Zhu, Andrew Tang,
532 De-An Huang, Yuke Zhu, and Anima Anandkumar. Minedojo: Building open-ended embodied
533 agents with internet-scale knowledge. *Advances in Neural Information Processing Systems*, 35:
534 18343–18362, 2022.

535 Siddhant Haldar, Vaibhav Mathur, Denis Yarats, and Lerrel Pinto. Watch and match: Supercharg-
536 ing imitation with regularized optimal transport. In *Conference on Robot Learning*, pp. 32–43.
537 PMLR, 2023.
538

539 Jonathan Ho and Stefano Ermon. Generative adversarial imitation learning. *Advances in neural*
information processing systems, 29, 2016.

- 540 Tao Huang, Guangqi Jiang, Yanjie Ze, and Huazhe Xu. Diffusion reward: Learning rewards via
541 conditional video diffusion. In *European Conference on Computer Vision*, pp. 478–495. Springer,
542 2024.
- 543 Julian Ibarz, Jie Tan, Chelsea Finn, Mrinal Kalakrishnan, Peter Pastor, and Sergey Levine. How to
544 train your robot with deep reinforcement learning: lessons we have learned. *The International
545 Journal of Robotics Research*, 40(4-5):698–721, 2021.
- 547 Andrew Jaegle, Yury Sulsky, Arun Ahuja, Jake Bruce, Rob Fergus, and Greg Wayne. Imitation
548 by predicting observations. In *International Conference on Machine Learning*, pp. 4665–4676.
549 PMLR, 2021.
- 550 Sergey Levine, Chelsea Finn, Trevor Darrell, and Pieter Abbeel. End-to-end training of deep visuo-
551 motor policies. *Journal of Machine Learning Research*, 17(39):1–40, 2016.
- 553 Minghuan Liu, Zhengbang Zhu, Yuzheng Zhuang, Weinan Zhang, Jianye Hao, Yong Yu, and Jun
554 Wang. Plan your target and learn your skills: Transferable state-only imitation learning via de-
555 coupled policy optimization. *arXiv preprint arXiv:2203.02214*, 2022.
- 556 Yuyang Liu, Weijun Dong, Yingdong Hu, Chuan Wen, Zhao-Heng Yin, Chongjie Zhang, and Yang
557 Gao. Imitation learning from observation with automatic discount scheduling. In *The Twelfth
558 International Conference on Learning Representations*, 2024.
- 560 Yecheng Jason Ma, Shagun Sodhani, Dinesh Jayaraman, Osbert Bastani, Vikash Kumar, and Amy
561 Zhang. Vip: Towards universal visual reward and representation via value-implicit pre-training.
562 *arXiv preprint arXiv:2210.00030*, 2022.
- 563 Yecheng Jason Ma, Joey Hejna, Chuyuan Fu, Dhruv Shah, Jacky Liang, Zhuo Xu, Sean Kirmani,
564 Peng Xu, Danny Driess, Ted Xiao, et al. Vision language models are in-context value learners. In
565 *The Thirteenth International Conference on Learning Representations*, 2024.
- 567 Ruiqian Nai, Jiacheng You, Liu Cao, Hanchen Cui, Shiyuan Zhang, Huazhe Xu, and Yang Gao.
568 Fine-tuning hard-to-simulate objectives for quadruped locomotion: A case study on total power
569 saving. *arXiv preprint arXiv:2502.10956*, 2025.
- 570 Ashvin Nair, Dian Chen, Pulkit Agrawal, Phillip Isola, Pieter Abbeel, Jitendra Malik, and Sergey
571 Levine. Combining self-supervised learning and imitation for vision-based rope manipulation. In
572 *2017 IEEE international conference on robotics and automation (ICRA)*, pp. 2146–2153. IEEE,
573 2017.
- 574 Andrew Y Ng, Daishi Harada, and Stuart Russell. Policy invariance under reward transformations:
575 Theory and application to reward shaping. In *Icml*, volume 99, pp. 278–287. Citeseer, 1999a.
- 577 Andrew Y Ng, Daishi Harada, and Stuart J Russell. Policy invariance under reward transforma-
578 tions: Theory and application to reward shaping. In *Proceedings of the Sixteenth International
579 Conference on Machine Learning*, pp. 278–287, 1999b.
- 580 Georgios Papagiannis and Yunpeng Li. Imitation learning with sinkhorn distances. In *Joint Eu-
581 ropean Conference on Machine Learning and Knowledge Discovery in Databases*, pp. 116–131.
582 Springer, 2022.
- 584 Deepak Pathak, Parsa Mahmoudieh, Guanghao Luo, Pulkit Agrawal, Dian Chen, Yide Shentu, Evan
585 Shelhamer, Jitendra Malik, Alexei A Efros, and Trevor Darrell. Zero-shot visual imitation. In
586 *Proceedings of the IEEE conference on computer vision and pattern recognition workshops*, pp.
587 2050–2053, 2018.
- 588 Alec Radford, Jong Wook Kim, Chris Hallacy, Aditya Ramesh, Gabriel Goh, Sandhini Agarwal,
589 Girish Sastry, Amanda Askell, Pamela Mishkin, Jack Clark, et al. Learning transferable visual
590 models from natural language supervision. In *International Conference on Machine Learning
591 (ICML)*, pp. 8748–8763. PMLR, 2021.
- 592 Ilija Radosavovic, Xiaolong Wang, Lerrel Pinto, and Jitendra Malik. State-only imitation learning
593 for dexterous manipulation. In *IROS*, 2021.

- 594 Aravind Rajeswaran, Vikash Kumar, Abhishek Gupta, Giulia Vezzani, John Schulman, Emanuel
595 Todorov, and Sergey Levine. Learning complex dexterous manipulation with deep reinforcement
596 learning and demonstrations. *arXiv preprint arXiv:1709.10087*, 2017.
- 597
- 598 João A Cândido Ramos, Lionel Blondé, Naoya Takeishi, and Alexandros Kalousis. Sample-efficient
599 on-policy imitation learning from observations. *arXiv preprint arXiv:2306.09805*, 2023.
- 600 Nicholas Roy, Ingmar Posner, Tim Barfoot, Philippe Beaudoin, Yoshua Bengio, Jeannette Bohg,
601 Oliver Brock, Isabelle Depatie, Dieter Fox, Dan Koditschek, et al. From machine learn-
602 ing to robotics: Challenges and opportunities for embodied intelligence. *arXiv preprint*
603 *arXiv:2110.15245*, 2021.
- 604 Pierre Sermanet, Corey Lynch, Yevgen Chebotar, Jasmine Hsu, Eric Jang, Stefan Schaal, Sergey
605 Levine, and Google Brain. Time-contrastive networks: Self-supervised learning from video. In
606 *2018 IEEE international conference on robotics and automation (ICRA)*, pp. 1134–1141. IEEE,
607 2018.
- 608
- 609 David Silver, Satinder Singh, Doina Precup, and Richard S Sutton. Reward is enough. *Artificial*
610 *intelligence*, 299:103535, 2021.
- 611
- 612 Chen Tang, Ben Abbatematteo, Jiaheng Hu, Rohan Chandra, Roberto Martín-Martín, and Peter
613 Stone. Deep reinforcement learning for robotics: A survey of real-world successes. In *Proceed-*
614 *ings of the AAAI Conference on Artificial Intelligence*, volume 39, pp. 28694–28698, 2025.
- 615 Gemini Team, Petko Georgiev, Ving Ian Lei, Ryan Burnell, Libin Bai, Anmol Gulati, Garrett Tanzer,
616 Damien Vincent, Zhufeng Pan, Shibo Wang, et al. Gemini 1.5: Unlocking multimodal under-
617 standing across millions of tokens of context. *arXiv preprint arXiv:2403.05530*, 2024.
- 618 Emanuel Todorov. Optimality principles in sensorimotor control. *Nature neuroscience*, 7(9):907–
619 915, 2004.
- 620
- 621 Faraz Torabi, Garrett Warnell, and Peter Stone. Behavioral cloning from observation. *arXiv preprint*
622 *arXiv:1805.01954*, 2018a.
- 623
- 624 Faraz Torabi, Garrett Warnell, and Peter Stone. Generative adversarial imitation from observation.
625 *arXiv preprint arXiv:1807.06158*, 2018b.
- 626 Cédric Villani et al. *Optimal transport: old and new*, volume 338. Springer, 2009.
- 627 Shengjie Wang, Shaohuai Liu, Weirui Ye, Jiacheng You, and Yang Gao. Efficientzero v2: Mastering
628 discrete and continuous control with limited data. *arXiv preprint arXiv:2403.00564*, 2024.
- 629
- 630 Donglai Wei, Joseph J Lim, Andrew Zisserman, and William T Freeman. Learning and using the
631 arrow of time. In *Proceedings of the IEEE conference on computer vision and pattern recognition*,
632 pp. 8052–8060, 2018.
- 633
- 634 Chao Yang, Xiaojian Ma, Wenbing Huang, Fuchun Sun, Huaping Liu, Junzhou Huang, and Chuang
635 Gan. Imitation learning from observations by minimizing inverse dynamics disagreement. *Ad-*
636 *vances in neural information processing systems*, 32, 2019.
- 637 Daniel Yang, Davin Tjia, Jacob Berg, Dima Damen, Pulkit Agrawal, and Abhishek Gupta.
638 Rank2reward: Learning shaped reward functions from passive video. In *2024 IEEE International*
639 *Conference on Robotics and Automation (ICRA)*, pp. 2806–2813. IEEE, 2024.
- 640
- 641 Denis Yarats, Rob Fergus, Alessandro Lazaric, and Lerrel Pinto. Mastering visual continuous con-
642 trol: Improved data-augmented reinforcement learning. *arXiv preprint arXiv:2107.09645*, 2021.
- 643
- 644 Tianhe Yu, Deirdre Quillen, Zhanpeng He, Ryan Julian, Karol Hausman, Chelsea Finn, and Sergey
645 Levine. Meta-world: A benchmark and evaluation for multi-task and meta reinforcement learning.
646 In *Conference on robot learning*, pp. 1094–1100. PMLR, 2020.
- 647

A APPENDIX

A.1 TASKS FOR EVALUATION

In this paper, we experiment with the following 10 tasks from the Meta-World suite (Yu et al., 2020):

1. **Button press topdown:** to press a button from the top.
2. **Door open:** to open a cabinet door with a handle.
3. **Window close:** to close a sliding window with a handle.
4. **Drawer open:** to open a cabinet drawer with a handle.
5. **Window open:** to open a sliding window with a handle.
6. **Stick push:** to pick up a stick and push a kettle with the stick.
7. **Disassemble:** to pick and remove a nut from a peg.
8. **Basketball:** to pick up a basketball and dump it into a basket.
9. **Lever pull:** to pull a lever up 90 degrees.
10. **Plate slide:** to push a plate into the goal area.

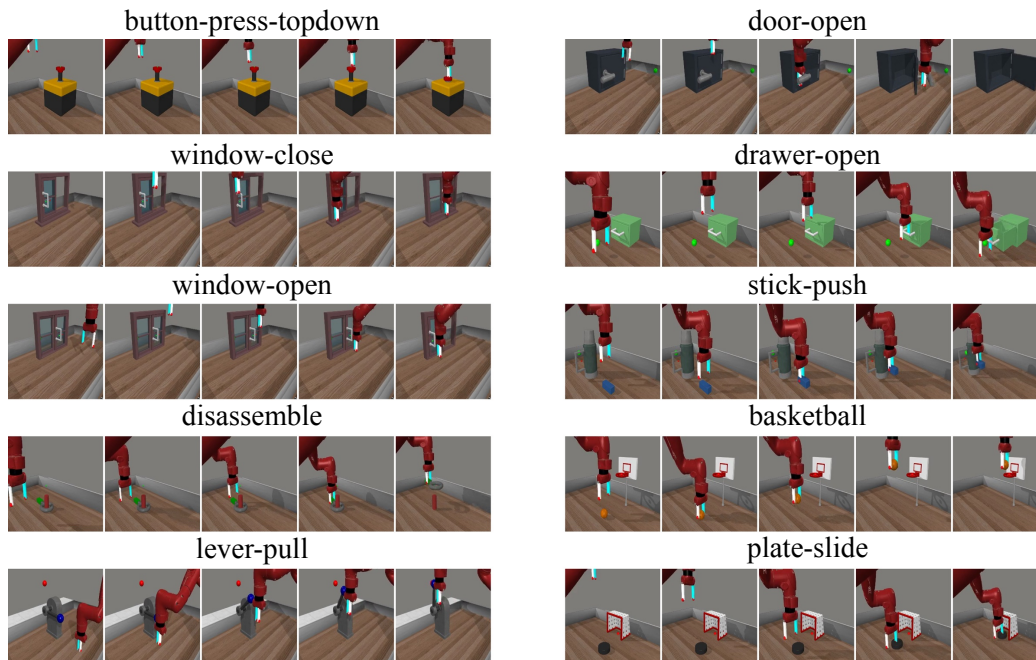
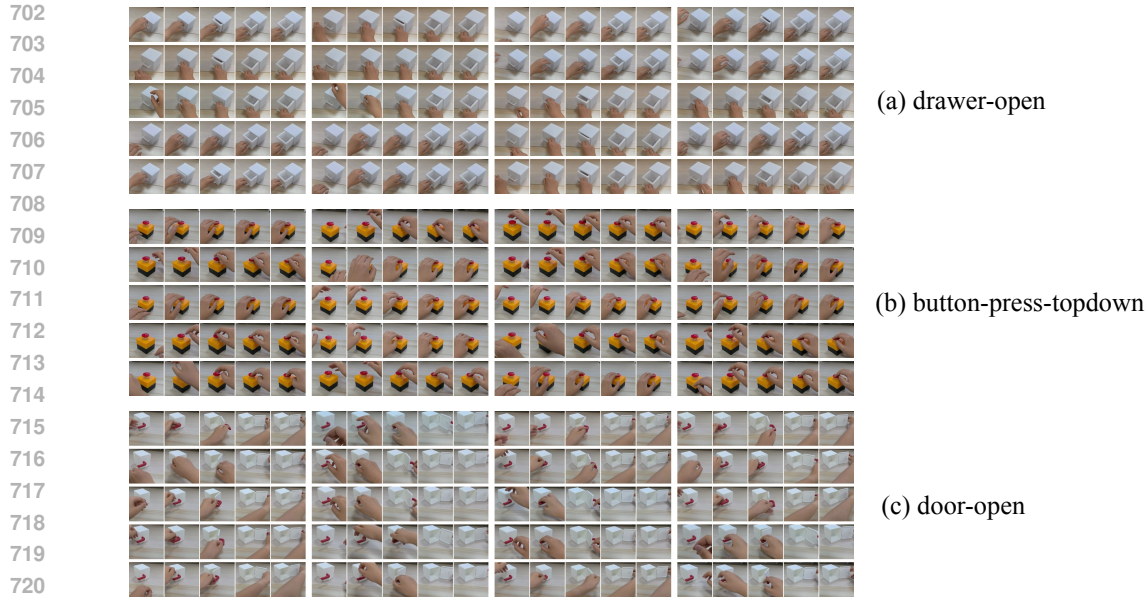


Figure 8: Meta-World tasks used in our paper.

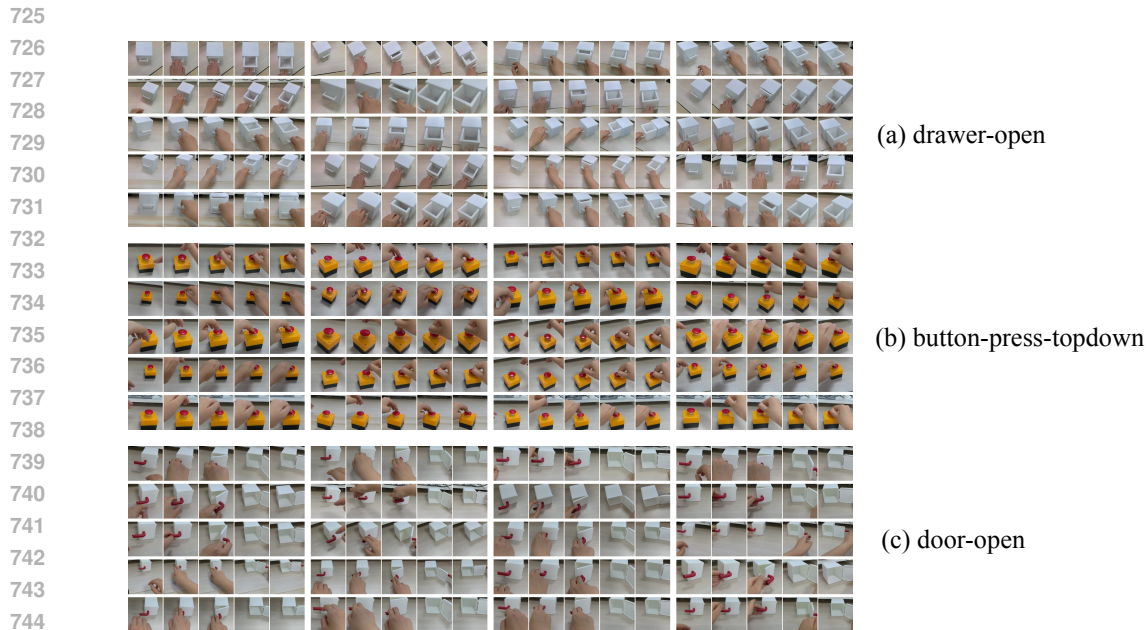
A.2 HUMAN VIDEO DATASETS FOR CROSS-DOMAIN EXPERIMENTS

This section presents the complete set of human videos used in the cross-domain experiments across three tasks. Each task includes 20 videos recorded in *single-view* (fixed viewpoint) and 20 videos recorded in *multi-view* (varying viewpoints) conditions. These videos differ from the robot setting in embodiment and background, and contain no action or state annotations.

The full set of videos for each task in both conditions is shown in Figure 9 and Figure 10.



723 Figure 9: Complete set of human videos recorded in the *single-view* condition for each of the three
724 tasks. Each task includes 20 videos captured from a fixed viewpoint.



747 Figure 10: Complete set of human videos recorded in the *multi-view* condition for each of the three
748 tasks. Each task includes 20 videos captured from varying viewpoints.

751 A.3 ADDITIONAL EXPERIMENT RESULTS

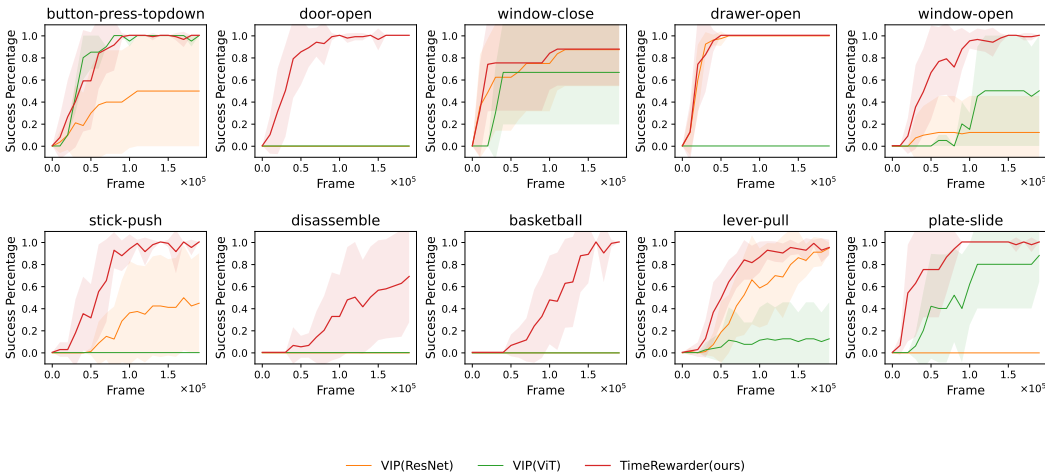
753 A.3.1 VIP BACKBONES

754 In the main experiments (Figure 5), we compare *TimeRewarder* with baseline methods including
755 Rank2Reward and PROGRESSOR, both of which use the same ViT backbone as *TimeRewarder*.

756 However, VIP originally uses a ResNet34 backbone as recommended by its codebase. To ensure a
 757 fair comparison, we re-train VIP using the same ViT backbone as *TimeRewarder*.
 758

759 As shown in Figure 11, the performance of VIP with ResNet34 versus ViT varies across different
 760 tasks. Sometimes, ResNet34 performs better, and other times, ViT shows superior performance.
 761 However, regardless of the backbone used, *TimeRewarder* consistently outperforms VIP across all
 762 tasks. This demonstrates that, while the choice of backbone can influence VIP’s performance on
 763 individual tasks, *TimeRewarder* remains more robust and superior in all scenarios.

764 This setup follows the same experimental conditions as in Section 5.1, where all methods, includ-
 765 ing VIP, are evaluated on the same 10 Meta-World manipulation tasks using sparse binary success
 766 signals.



783 Figure 11: VIP performance with ResNet34 vs. ViT backbones across tasks. The results show that
 784 *TimeRewarder* outperforms VIP regardless of the backbone used. All methods are evaluated with
 785 reinforcement learning using sparse environment success signals and dense proxy rewards. Curves
 786 show the mean \pm s.d. over eight seeds.
 787

789 A.3.2 RL WITH ONLY PROXY REWARD

791 Compared to Figure 5, Figure 12 presents the results when the environment’s sparse reward is en-
 792 tirely removed, relying solely on the learned proxy reward. Additionally, we include results for the
 793 ILfO baseline **BCO** (Torabi et al., 2018a; Baker et al., 2022). Under the constraint of extremely
 794 short training (only 200,000 frames), no successes are achieved. However, by the end, the agent has
 795 started making progress and completing part of the task, though not the full goal.
 796

797 A.3.3 CHOICE OF REWARD COMBINATION FACTOR

798 In equation 7 we use a weight constant α to align the scales of the dense and sparse components so
 799 that neither term dominates purely due to magnitude differences, since different methods produce
 800 reward functions on different scales. In practice, we use an adaptive way to choose α , which is to
 801 calculate the maximum value of the dense reward for the first few trajectories, and then set α to ten
 802 times this maximum value.
 803

804 Figure 13 further shows that the performance of *TimeRewarder* is not sensitive to the value of α .
 805

806 A.3.4 CHOICE OF DISCRETIZATION BINS

807 Figure 14 shows the performance of *TimeRewarder* with different bin number K in 2-hot dis-
 808 cretization. While the default $K = 20$ represents a practical tradeoff between reward precision and
 809 optimization stability, the performance is not very sensitive to the value of K .

810
811
812
813
814
815
816
817
818
819
820
821
822
823
824
825
826
827
828
829
830
831
832
833
834
835
836
837
838
839
840
841
842
843
844
845
846
847
848
849
850
851
852
853
854
855
856
857
858
859
860
861
862
863

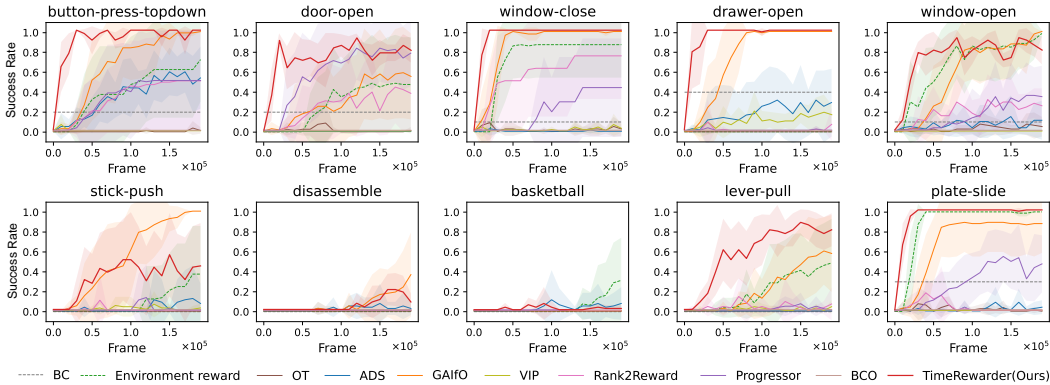


Figure 12: Reinforcement learning without sparse reward. Curves show mean \pm s.d. over eight seeds. Dashed lines indicate behavior cloning (BC) and environment dense reward supervision.

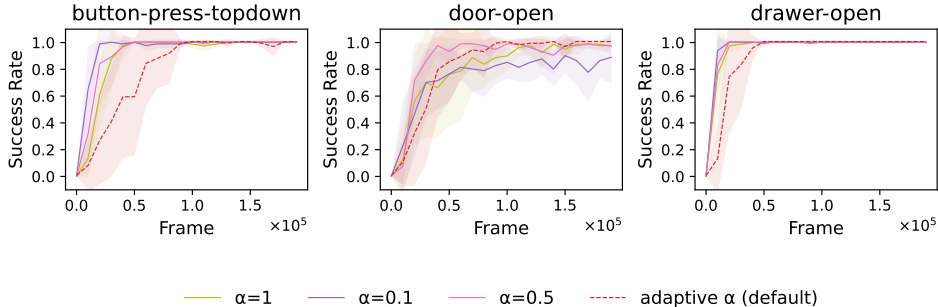


Figure 13: *TimeRewarder*'s performance with different α . Curves show mean \pm s.d. over eight seeds.

A.3.5 ADDITIONAL CROSS-DOMAIN EXPERIMENTS

In the main experiment results, with 100 Meta-World demonstrations, performance is already strong. Adding 20 human videos yields similar performance but slightly improves sample efficiency by further broadening the coverage. The results are shown in Figure 15 .

A.3.6 TRAINING FROM SCRATCH

Figure 16 presents an ablation study in which a ViT-B model trained from scratch is used as the visual backbone, replacing the CLIP-pretrained ViT-B employed in the main experiments. We compare *TimeRewarder* against the baseline methods Rank2Reward and PROGRESSOR. As expected, the absolute performance decreases due to the weaker visual representations. Nevertheless, the overall trends persist, and *TimeRewarder* continues to outperform the baseline methods.

A.4 IMPLEMENTATION DETAILS

A.4.1 ALTERNATIVE TEMPORAL MODELING APPROACHES

In our main method, *TimeRewarder* does temporal modeling through predicting the relative progress between two frames in a video. We also examined other three temporal modeling approaches as following.

(1) only from init. Considering the distribution shift, predicting the progress from each frame in an agent's rollout trajectory to a goal image derived from another expert trajectory may not be suitable. In addition to the goal frame, a natural choice is to use the initial frame as an anchor, which captures the positions of objects in the environment. In this context, when sampling frame pairs from expert trajectories, instead of randomly selecting any two frames, we fix the first frame as the initial frame.

864
865
866
867
868
869
870
871
872
873
874
875
876
877
878
879
880
881
882
883
884
885
886
887
888
889
890
891
892
893
894
895
896
897
898
899
900
901
902
903
904
905
906
907
908
909
910
911
912
913
914
915
916
917

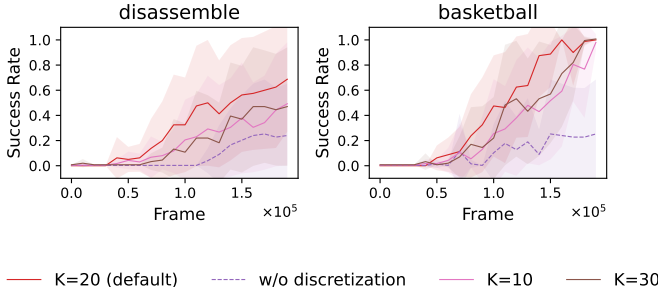


Figure 14: *TimeRewarder*'s performance with different bin number K in 2-hot discretization. Curves show mean \pm s.d. over eight seeds.

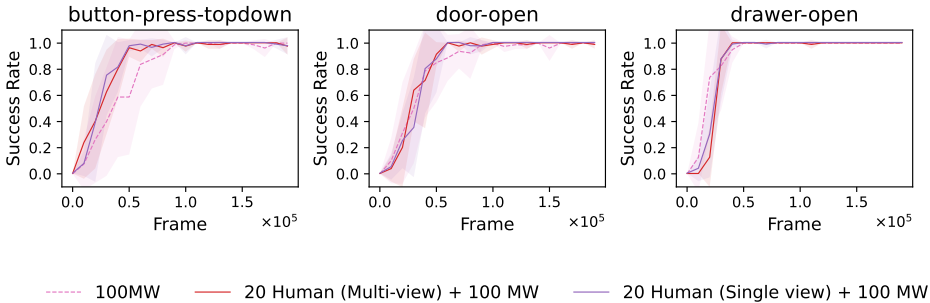


Figure 15: Cross-domain experiment results of adding 20 human videos to 100 Meta-World demonstrations. Curves show mean \pm s.d. over eight seeds.

We then predict the progress within the range of $[0, 1]$, while adhering to the three methodological components in *TimeRewarder*.

(2) single frame input. The simplest method to capture temporal information in a video is to directly predict the normalized temporal position (ranging from $[0,1]$) of each individual frame. In contrast to *TimeRewarder*, we use only one frame as input for our reward model instead of two. We uniformly sample the frame and apply the discretization technique.

(3) order prediction. Our order prediction setting is inspired by the setup of GVL (Ma et al., 2024). During training, we uniformly sample $n = 32$ frames from each expert video and apply a random permutation. The model is trained to recover the original ordering using a cross-entropy loss over permutation positions. At test time, we input an agent trajectory and predict a score for each frame reflecting its position in the estimated order. The model architecture mirrors that of *TimeRewarder*, but replaces the temporal regression head with a frame-wise classifier for permutation indices. Specifically, the predicted scalar values are normalized between $[-1, 1]$.

Reward computation: For all three methods mentioned above, the prediction of the reward model reflects the progress of an agent's trajectory at each time step. These scores are then utilized as potentials in a potential-based reward formulation. Consequently, the reward for each step is defined as the forward difference between successive predicted values.

A.4.2 DEMONSTRATION COLLECTION FOR META-WORLD

To better approximate in-the-wild video data, we collected Meta-World demonstrations under a deliberately diverse initialization protocol. Rather than using the default narrow initialization range, where both agents and experts begin from nearly identical configurations, we expanded the initial state space to cover a broad variety of robot and object positions. This leads to demonstrations with much greater appearance diversity and prevents agent trajectories from being trivially aligned to demonstrations at the pixel level.

This choice also explains the results in Figure 5, where occupation-matching methods such as Optimal Transport (OT) and its extension ADS perform poorly. With the default narrow initialization,

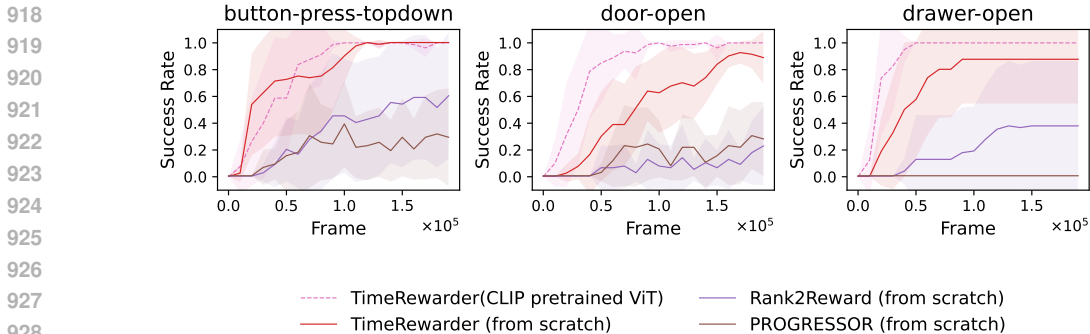


Figure 16: Ablation study with from-the-scratch ViT-B as the vision backbone. Curves show mean \pm s.d. over eight seeds.

agents and experts share similar starting conditions, allowing OT and ADS to exploit appearance-level shortcuts when aligning trajectories. Once the initialization range is broadened, these shortcuts disappear, and the assumptions underpinning OT and ADS no longer hold, leading to degraded performance.

Crucially, this setting more faithfully reflects real-world conditions, where demonstrations and agent experiences seldom begin from the same initial states. It therefore underscores the importance of methods like *TimeRewarder* that extract robust progress signals rather than depending on superficial appearance matching.

A.4.3 HYPERPARAMETERS

For reward learning, we use a ViT-B/16 backbone. Frame features are extracted, concatenated into a 1024-dimensional vector, and projected through a linear layer into 20 discretized bins. Training data is augmented to 10,000 pairs per epoch. The hyperparameters are summarized in Table 1.

Table 1: Reward model hyperparameters.

Config	Value
Backbone	ViT-B/16
Feature dimension	1024(512 \times 2)
Output bins	20 (two-hot discretization)
Training pairs per epoch	10,000
Epochs	100
Warm-up epochs	5
Batch size	16
Accumulation steps	1
Optimizer	Adam
Learning rate	2×10^{-5}

We equip all the methods with the same underlying RL algorithm, DrQ-v2 (Yarats et al., 2021). The hyperparameters are listed in Table 2.

972
973
974
975
976
977
978
979
980
981
982
983
984
985
986
987
988
989
990
991
992
993
994
995
996
997
998
999
1000
1001
1002
1003
1004
1005
1006
1007
1008
1009
1010
1011
1012
1013
1014
1015
1016
1017
1018
1019
1020
1021
1022
1023
1024
1025

Table 2: RL hyperparameters.

Config	Value
Replay buffer capacity	150000
n -step returns	3
Mini-batch size	512
Discount	0.99
Optimizer	Adam
Learning rate	10^{-4}
Critic Q-function soft-update rate τ	0.005
Hidden dimension	1024
Exploration noise	$\mathcal{N}(0, 0.4)$
Policy noise	$\text{clip}(\mathcal{N}(0, 0.1), -0.3, 0.3)$
Delayed policy update	1